

THE SPATIAL DISTRIBUTION OF GALAXIES OF DIFFERENT SPECTRAL TYPES IN THE MASSIVE INTERMEDIATE-REDSHIFT CLUSTER MACSJ0717.5+3745*

CHENG-JIUN MA, HARALD EBELING, DAVID DONOVAN, AND ELIZABETH BARRETT
Institute for Astronomy, University of Hawaii, 2680 Woodlawn Drive, Honolulu, HI 96822, USA
Draft version November 14, 2018

ABSTRACT

We present the results of a wide-field spectroscopic analysis of the galaxy population of the massive cluster MACSJ0717.5+3745 and the surrounding filamentary structure ($z=0.55$), as part of our systematic study of the 12 most distant clusters in the MACS sample. Of 1368 galaxies spectroscopically observed in this field, 563 are identified as cluster members; of those, 203 are classified as emission-line galaxies, 260 as absorption-line galaxies, and 17 as E+A galaxies (defined by $\frac{H_\delta+H_\gamma}{2} > 6\text{\AA}$ and no detection of [OII] and H_β in emission). The variation of the fraction of emission- and absorption-line galaxies as a function of local projected galaxy density confirms the well-known morphology-density relation, and becomes flat at projected galaxy densities less than $\sim 20\text{Mpc}^{-2}$. Interestingly, 16 out of 17 E+A galaxies lie (in projection) within the ram-pressure stripping radius around the cluster core, which we take to be direct evidence of ram-pressure stripping being the primary mechanism that terminates star-formation in the E+A population of galaxy clusters. This conclusion is supported by the rarity of E+A galaxies in the filament which rules out galaxy mergers as the dominant driver of evolution for E+A galaxies in clusters. In addition, we find the 42 e(a) and 27 e(b) member galaxies, i.e., the dusty-starburst and starburst galaxies respectively, to be spread out across almost the entire study area. Their spatial distribution, which shows a strong preference for the filament region, suggests that starbursts are triggered in relatively low-density environments as galaxies are accreted from the field population.

Subject headings: Galaxy: evolution, Galaxy:formation, galaxies:clusters:general, techniques:spectroscopic

1. INTRODUCTION

It is widely accepted that the effect of environment is one of the most important factors for galaxy evolution. Unlike field galaxies for which the dominant physical mechanism driving evolution is galaxy-galaxy mergers, as has been revealed in many large-scale surveys (Gomez et al. 2003; Lewis et al. 2003; Cooper et al. 2007), cluster galaxies evolve in a more complex fashion (see, e.g., the review by Bower & Balogh (2004)). As a result, cluster galaxies behave differently from field galaxies at the same epoch. One of the best-studied examples of this difference between the properties of galaxies in clusters and in the field is the morphology-density relation (Oemler 1974; Dressler 1980), i.e., the fact that the fraction of late-type galaxies drops precipitously toward the center of a cluster, whereas the fraction of early-type galaxies increases dramatically. In addition, the Butcher-Oemler effect (Butcher & Oemler 1978), which states that galaxies in rich clusters tend to be bluer and more active (i.e. feature emission lines) with increasing cluster redshift out to at least $z \sim 0.8$, implies that the build-up of the morphology-density

relation is still ongoing at redshifts less than unity. Therefore, much effort (Couch & Sharples 1987; Dressler et al. 1997; Poggianti et al. 1999; Smith et al. 2005; Postman et al. 2005; Moran et al. 2006; Tran et al. 2007) has gone into establishing whether and, if so, how blue late-type galaxies are transformed into early-type galaxies, specifically S0 galaxies.

Clusters at intermediate redshift ($z \sim 0.5$) provide us with a unique opportunity to examine this hypothesized transformation as well as the dominant physical mechanisms driving it. Recent work in this field includes a study of the morphological distribution of galaxies in the cluster Cl0024+16 at $z = 0.39$ (Treu et al. 2003), and a comparison of the spatial distribution and spectroscopic properties of spiral galaxies with quenched star formation (passive spirals) and newly formed S0 galaxies in, again Cl0024+16, as well as in the more massive system MS0451.6–0305 at $z = 0.55$ (Moran et al. 2007). The authors of these studies suggest that ram-pressure stripping (Gunn & Gott 1972) is not the only mechanism involved in building up the population of S0 galaxies from late-type galaxies, although it does accelerate the process. The transformation is actually initiated much farther away from the cluster center, and at a slower pace, by the processes of strangulation (Larson et al. 1980) or galaxy-galaxy harassment (Moore et al. 1996). Additional evidence of this evolution from blue late-type galaxies to S0 galaxies is presented by Tran et al. (2007) who, using the spectroscopic diagnostics H_δ and $D_n(4000)$ (Kauffmann et al. 2003) in their study of the cluster MS1054.4–0321 ($z = 0.823$), confirms that S0 galaxies in the cluster are, in general, younger than the elliptical galaxies. Tran et al. (2007) suggest that these S0 galaxies have recently been converted from late-type galaxies falling in from the field (see also Tran et al. (2005)).

To improve our understanding of the different physical effects governing galaxy evolution from the cluster out-

*BASED IN PART ON DATA COLLECTED AT SUBARU TELESCOPE, WHICH IS OPERATED BY THE NATIONAL ASTRONOMICAL OBSERVATORY OF JAPAN. BASED ALSO, IN PART, ON OBSERVATIONS OBTAINED WITH MEGAPRIME/MEGACAM, A JOINT PROJECT OF CFHT AND CEA/DAPNIA, AT THE CANADA-FRANCE-HAWAII TELESCOPE (CFHT) WHICH IS OPERATED BY THE NATIONAL RESEARCH COUNCIL (NRC) OF CANADA, THE INSTITUTE NATIONAL DES SCIENCES DE L'UNIVERS OF THE CENTRE NATIONAL DE LA RECHERCHE SCIENTIFIQUE OF FRANCE, AND THE UNIVERSITY OF HAWAII. THE SPECTROSCOPIC DATA PRESENTED HEREIN WERE OBTAINED AT THE W.M. KECK OBSERVATORY, WHICH IS OPERATED AS A SCIENTIFIC PARTNERSHIP AMONG THE CALIFORNIA INSTITUTE OF TECHNOLOGY, THE UNIVERSITY OF CALIFORNIA AND THE NATIONAL AERONAUTICS AND SPACE ADMINISTRATION. THE OBSERVATORY WAS MADE POSSIBLE BY THE GENEROUS FINANCIAL SUPPORT OF THE W.M. KECK FOUNDATION.

skirts to the cluster core, we have embarked on an extensive magnitude-limited wide-field spectroscopic survey of the galaxy population of 12 clusters with redshifts above 0.5, selected from the MAAssive Cluster Survey (MACS) (Ebeling et al. 2004, 2007). In this paper we present results from our pilot study of MACSJ0717.5+3745 ($z = 0.545$). MACSJ0717.5+3745, which has the most extensive spectroscopic data set of these 12 at present, features a complex X-ray morphology in the cluster core as well as a giant filament described by Ebeling et al. (2004). We here focus on the spectroscopic analysis and classification of galaxies in MACSJ0717.5+3745, with special emphasis on E+A galaxies, a galaxy type that, as shall be explained in the following section, holds great promise as a diagnostic for cluster-related mechanisms of galaxy evolution.

This paper is organized as follows. In §2, we review the properties of E+A galaxies. In §3, we describe the data used for this study and give an overview of the data reduction procedure. In §4 we discuss the selection of the cluster members used in our analysis, and describe the equivalent-width measurement and spectral classification. In §5, we present results based on the spatial distribution of each spectral type of galaxies. In §6 we interpret our findings; a conclusion is given in §7. Throughout this paper, we adopt the concordance Λ CDM cosmology with $h_0 = 0.7$, $\Omega_\lambda = 0.7$, $\Omega_m = 0.3$. Magnitudes are quoted in the AB system.

2. E+A GALAXIES

One of the most promising approaches to understanding how blue and active late-type galaxies are transformed into red and passive early-type systems (Bower & Balogh 2004) is through studies of galaxies caught in transition between the two types, for example E+A galaxies (Dressler & Gunn 1983), also called k+a, a+k, or post-starburst galaxies. Although there is no unique definition of this transition type, its representatives are characterized by the presence of strong Balmer absorption lines in their spectra, indicating a large fraction of A-type stars, and weak or no ongoing star formation, often quantified by the strength of the [OII] emission line. Since the duration of the E+A phase is relatively short (less than 1 Gyr) E+A galaxies should be good tracers of the environment that is host to a critical part of the evolution of galaxies in clusters.

Although E+A galaxies were first found in clusters at intermediate redshift (e.g., Dressler & Gunn 1983, Couch & Sharples 1987), their origin and habitat was soon proven to be more varied by the discovery that the majority of E+A galaxies in the local universe are in fact not located in dense environments (Zabludoff et al. 1996; Goto et al. 2003; Goto 2007; Hogg et al. 2006; Quintero et al. 2004). As for the possible physical origin of this type of galaxies, Zabludoff et al. (1996) and Yang et al. (2004) report that many of the E+A galaxies in the field show evidence of galaxy mergers. At higher redshift, however, E+A galaxies are predominantly found in the much denser environment of clusters (Tran et al. 2003, 2004), which have thus been suspected of being instrumental in the termination of star-formation activity in these systems. In addition, Poggianti et al. (2004) show that, at $M_v > -18.5$, the post-starburst galaxies in Coma are fainter than the typical E+A galaxies found in clusters at higher redshift, which suggests that the evolution of post-starburst galaxies follows the "downsizing" trend proposed by Cowie et al. (1996). Any discrepancies between the properties of E+A galaxies in the local field and in intermediate-redshift clusters may thus be

explained by the combination of evolution and selection biases, in the sense that the local surveys sample predominantly luminous galaxies and hence do not probe the population of fainter E+A galaxies in clusters (the faintest E+A galaxy in Zabludoff et al. (1996) features $M_R \sim -18.5$, whereas the magnitude limit in Goto et al. (2003) is $M_r < -21.84$).

Unlike previous studies (Tran et al. 2003, 2004; Goto et al. 2003), the goal of this work is not the issue of whether E+A galaxies are more likely to be found in clusters or in the field; rather, we focus on the spatial distribution of E+A galaxies around the massive cluster MACSJ0717.5+3745 to isolate the most probable physical mechanism responsible for their creation in a cluster environment. In this context we also attempt to address the question of the origin of the E+A population by investigating the spatial distribution of possible star-burst galaxies, the so-called e(a) and e(b) galaxies (Dressler et al. 1999; Poggianti & Wu 2000).

3. DATA AND ANALYSIS

Using optical images obtained with the Suprime-Cam wide-field camera on the Subaru 8m telescope on Mauna Kea (Miyazaki et al. 2002), we identify galaxies within the 34×27 arcmin² Suprime-Cam field of view. We then employ color selection to obtain spectra of a subset of presumed cluster members, primarily using the DEep Imaging Multi-Object Spectrograph (DEIMOS) on the Keck-II 10m telescope. In order to study the spectroscopic properties of galaxies in different environments, the DEIMOS masks are designed to cover the entire cluster including the filament and a satellite cluster. We use the spectroscopic data to determine the redshift of galaxies, as well as their spectral types. We follow the spectral classification scheme of Tran et al. (2003) (with some modifications) to categorize the cluster galaxies into emission-line, absorption-line, and E+A galaxies. The emission-line galaxies can be further subdivided into e(a), e(b), and e(c) galaxies according to the equivalent width of the H_δ absorption and [OII] emission lines (Dressler et al. 1999). Complementing our optical analysis of the galaxy population of this system, X-ray data obtained with the imaging array of the Chandra Advanced CCD Imaging Spectrometer (ACIS-I) are analyzed to provide a basic model of the gaseous intracluster medium.

3.1. Optical Photometry

We use images in the B, V, R_c , I_c , and z' bands obtained with Suprime-Cam, supplemented by images in the u^* band obtained with the MegaPrime camera on the CFHT 3.6m telescope. The observations were performed from December 2000 to February 2004. All data are reduced employing standard techniques, which have, however, been adapted to deal with the special characteristics of the Suprime-Cam and MegaPrime data; details are given by Donovan (2007).

In order to allow a robust estimate of the spectral energy distribution (SED) to be obtained for all objects within the field of view, the imaging data from the various passbands are seeing-matched using the technique described in Kartaltepe et al. (2008); this ensures that the images for all bands have the same effective spatial resolution of $1''$.

Object catalogues are then created with SExtractor version 2.4.3 (Bertin & Arnouts 1996) in "dual image" mode with the R-band image as the reference detection image. We separate stars from galaxies by fitting the stellar sequence in the distributions of magnitude vs peak surface-brightness, and magnitude vs half-light radius. Isophotal galaxy magnitudes calculated for elliptical apertures are returned by SExtractor in the

MAG_AUTO parameter. The photometric calibration of the Suprime-Cam imaging data is performed by means of a snapshot observation of a nearby SDSS field¹ and uses hundreds of stars with magnitudes ranging from 16 mag to 18 mag. The calibration of our MegaCam data is supplied by CFHT’s Elixir project².

3.2. X-ray Data

The X-ray data are used to derive global cluster properties, most importantly the virial radius and the ram-pressure stripping radius. To this end, we analyze the data taken with the Chandra ACIS-I instrument in January 2003 with a total exposure time of 60 ks (ObsID 4200). The data reduction is performed following the procedure described by Ruderman et al. (2005). Fig. 1 shows the adaptively smoothed X-ray emission in the 0.5–7 keV band as observed by ACIS-I. The X-ray luminosity and temperature are listed in Table 5; a dynamical analysis based on the X-ray properties and the velocity dispersion will be presented in §5.3.

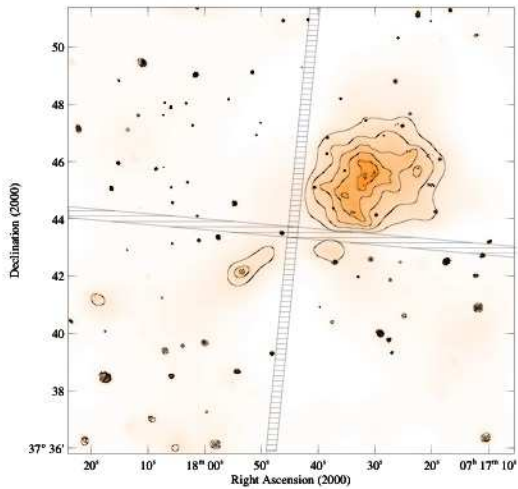


FIG. 1.— X-ray emission in the field of MACSJ0717.5+3745 as observed with Chandra’s ACIS-I detector in the 0.5–7 keV band. The shown image has been adaptively smoothed using the *asmooth* algorithm (Ebeling et al. 2006) requiring a minimal significance with respect to the local background of 99%. The shaded cross marks the regions falling onto the chip gaps of the ACIS-I detector. A close-up view of the cluster core based on the same X-ray data has been previously published by Ebeling et al. (2007). [The full resolution figure will be published in ApJ]

3.3. Optical Spectroscopy

MACSJ0717.5+3745 has the most extensive spectroscopic data in our on-going follow-up study of the dynamical structure and galaxy properties in 12 clusters with $z > 0.5$ in the MACS sample (Ebeling et al. 2007; Kartaltepe et al. 2008). The spectroscopic data set used here is compiled primarily from the observation of 18 masks with the DEIMOS spectrograph on the Keck-II telescope. In addition, some spectra obtained using the Low Resolution Image Spectrometer (LRIS) on the Keck-I telescope, and the Gemini Multi-Object Spectrographs (GMOS) on the Gemini telescope are included.

¹ The SDSS photometry is transformed into the Johnson-Cousin system using the equation of Lupton (2005) provided on <http://www.sdss.org/dr5/algorithms/sdssUBVRITransform.html>.

² <http://www.cfht.hawaii.edu/Instruments/Elixir/>

TABLE 1
SUMMARY OF SPECTROSCOPIC OBSERVATIONS

Instrument	Date	Grating	λ_c (Å)	Filter	Total Exposure Time (sec)
LRIS ^a	2000-11-20	600/7500	6200	GC495	3600
LRIS ^a	2000-11-20	600/7500	6200	GC495	4800
LRIS ^a	2000-11-21	600/7500	6200	GC495	3600
LRIS ^a	2002-11-29	600/7500	6500	GC495	5400
LRIS ^a	2002-11-29	600/7500	6500	GC495	6000
GMOS-N ^a	2004-03-12	B600	6700	GC455	5400
DEIMOS ^a	2003-12-23	600ZD	6500	GC455	7200
DEIMOS ^a	2004-12-16	600ZD	7000	GC455	5400
DEIMOS ^a	2004-12-16	600ZD	7000	GC455	5400
DEIMOS ^a	2004-12-16	600ZD	7000	GC455	5400
DEIMOS ^a	2005-02-12	600ZD	7000	GC455	3239
DEIMOS ^a	2005-02-12	600ZD	7000	GC455	6900
DEIMOS	2006-12-22	600ZD	6300	GC455	5400
DEIMOS	2006-01-31	600ZD	6300	GC455	6047
DEIMOS	2006-01-31	600ZD	6300	GC455	5400
DEIMOS	2006-01-31	600ZD	6300	GC455	5400
DEIMOS	2006-01-31	600ZD	6300	GC455	4991
DEIMOS	2006-02-01	600ZD	6300	GC455	5400
DEIMOS	2006-02-01	600ZD	6300	GC455	3600
DEIMOS	2006-02-01	600ZD	6300	GC455	5400
DEIMOS	2006-02-01	600ZD	6300	GC455	3600
DEIMOS	2008-01-05	600ZD	6300	GC455	5400
DEIMOS	2008-01-06	600ZD	6300	GC455	5400
DEIMOS	2008-01-07	600ZD	6300	GC455	5400

^a Reference: Barrett (2005)

The instrumental configuration of these observations is summarized by Barrett (2005), from where we have extracted the essential information listed in Table 1. The chosen setup is a compromise between the requirements of wavelength coverage from the [OII] $\lambda\lambda 3727$ line to the H_β line at a redshift of about 0.5, and moderately high spectral resolution. After reducing the spectra using the standard DEIMOS pipeline developed by the DEEP2 team, the redshifts are determined and verified manually using at least two prominent spectral features, such as (in absorption) Calcium H and K, H_δ , or the G band, and (in emission) [OII] $\lambda\lambda 3727$, H_β , and [OIII] $\lambda\lambda 4959, 5007$. Based on repeated observations of individual objects, we estimate the error in the resulting redshifts to be about 70 km/s, which is consistent with the spectral resolution of the observations.

The final spectroscopic catalogue comprises 1103 galaxies, of which 563 are cluster members (Table 3). Fig. 2 shows the location of the spectroscopically observed objects within our study region which is highlighted by the outline of the DEIMOS masks. The full redshift distribution is shown in Fig. 3. Cluster membership is assigned to all galaxies with $0.522 < z < 0.566$, the redshift range given by $z = z_{cl} \pm 2.5\sigma$, where the cluster redshift $z_{cl} = 0.5446$ and velocity dispersion $\sigma = 1612 \text{ km s}^{-1}$ (Table 5) are determined from the redshift distribution of galaxies within the virial radius of the cluster (Ebeling et al. 2007). The final catalogue, including redshifts and equivalent widths of the spectral features ([OII], H_δ , H_γ , $D_n(4000)$, H_β , and [OIII]), will be published in a separate data paper.

4. SPECTROSCOPIC ANALYSIS

4.1. Object Selection and Completeness

Since it is impractical to cover the entire sample of galaxies spectroscopically from the cluster core to the outskirts, we had to select targets in a way that increases the efficiency of cluster member detections while minimizing any potential bias. Since, at the time this project started, we did not have imaging

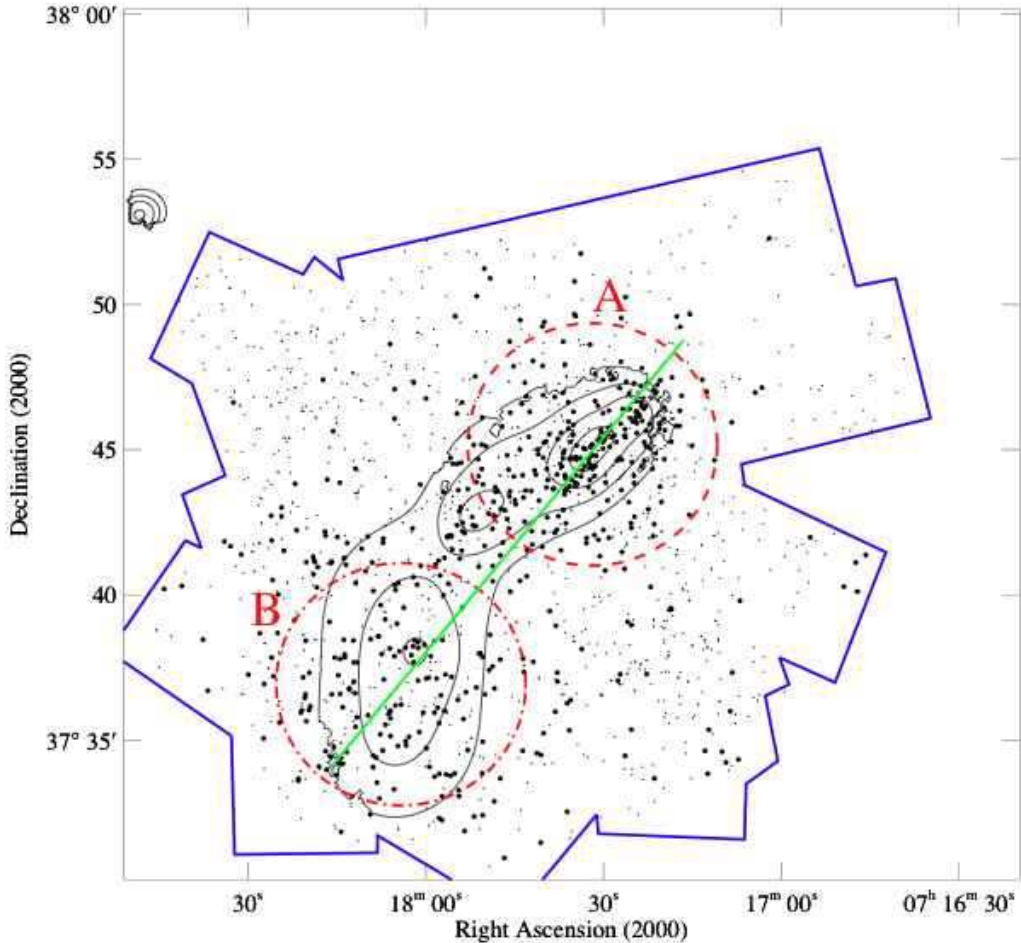


FIG. 2.— Spatial distribution of galaxies observed spectroscopically: small dots mark the location of all sources with measured spectrum, large dots mark confirmed cluster members. The overlaid contours show the projected galaxy density as computed by *asmooth* (Ebeling et al. 2006). An image of the distribution of all galaxies in the photometric redshift catalogue (§5.1) is adaptively smoothed such that all features in the smoothed image are 3σ significant with respect to the local background, where feasible. The plotted contours are located at 17, 35, 71, 142, and 285 Mpc^{-2} , respectively; they are truncated where the significance of the signal is less than 3σ . The blue boundary indicates the outline of all DEIMOS masks and defines the study region for this paper. All areas observed with GMOS and LRIS are covered by the DEIMOS masks. The two red circles (1.6 Mpc radius) indicate two regions of particular interest which will be discussed in more detail in §5.4 and §5.6: (a) the center of the cluster (dashed), and (b) the endpoint of the filament (dash-dotted). Both of these regions contain a local peak of the galaxy density. The green line crudely describes the large-scale orientation of the overall system and will be used in §5.3 to assess how galaxy properties vary as a function of environment. [The full resolution figure will be published in ApJ]

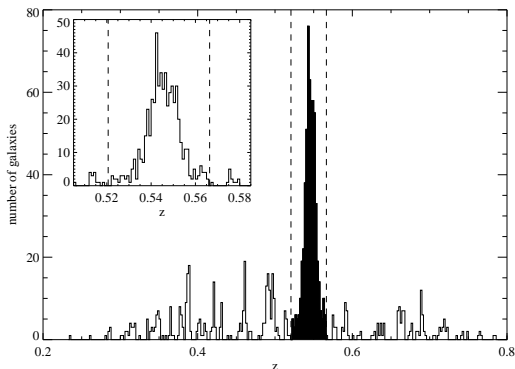


FIG. 3.— Redshift distribution for all spectroscopically observed galaxies. The systemic redshift of MACSJ0717.5+3745 is found to be $z_{cl} = 0.545$. The dashed lines at $z = 0.522$ and $z = 0.566$ ($z = z_{cl} \pm 3\sigma$) mark the spectroscopic extent of the cluster; the black area highlights the cluster members. A zoomed-in view of the redshift range near the cluster redshift is shown in the sub-panel.

data in a sufficient number of bandpasses to determine credible photometric redshifts, the target list for our spectroscopic observations is selected using the color magnitude diagram for the V and R_c filters (Fig. 4), making use of the cluster red sequence. To maximize completeness, we limit our survey to relatively bright objects ($m_{R_c} \leq 22.25$, which is, equivalently, $M_{R_c} \leq M^* + 2$ at $z=0.55$) while adopting a generous color cut toward the blue end of the distribution. The latter was adjusted in the course of the survey such that its locus coincides with the V- R_c color (relative to the red sequence) at which the fraction of galaxies found to be cluster members falls below 20% (Fig. 5). However, there will be unavoidably a few extremely blue galaxies that are in fact cluster members but do not satisfy our selection criteria. We estimate the resulting incompleteness by fitting a heuristic Gaussian model to the data shown in Fig. 5. If we assume that the probability derived from the observed sample is representative, and that the Gaussian fit can be extrapolated to yet bluer colors, we would expect our survey to be incomplete at the $\sim 2\%$ level. We note, however, that this incompleteness is severely

color-dependent which, as we will show in §5.2, could potentially cause the fraction of emission-line galaxies, but not the fraction of E+A galaxies, to be significantly underestimated.

We define the completeness of our spectroscopic survey as the ratio of the number of sources observed to the number of sources in the photometric catalogue (within the color band marked in Fig. 4), including spectra from which we failed to measure a redshift³. In addition we define the efficiency of our survey as the ratio of the number of high-quality spectra, from which both the redshift and the equivalent width of spectral features can be measured accurately (again within the color limits marked in Fig. 4). The completeness and efficiency as a function of galaxy magnitude are shown in the top panel of Fig. 6. Inside the entire study region, the completeness is roughly constant at about 70% at $R_c < 21.75$, with the curve only dropping within the very last bin before the magnitude limit at $R_c = 22.25$. Also shown in the top panel of Fig. 6 is the completeness within a radius of 2 Mpc from the center of the cluster: again the completeness is roughly independent of magnitude (except for the final bin before our global magnitude limit) but now at a much higher level near unity. Although the difference between these two curves shows that the completeness of our survey is not spatially uniform, the relative spatial distribution of galaxies of different types should be unaffected.

The bottom panel in Fig. 6 shows the efficiency in determining the galaxy redshift and the efficiency for spectroscopic classification. The former is almost perfect over the full magnitude range. The criteria used to classify galaxies according to spectral type (defined in the following two sections) are much stricter; still, the efficiency for spectroscopic classification remains better than 0.8 at all magnitudes, reflecting the good signal-to-noise ratio of most of our spectra. Only a handful of spectra feature very low signal-to-noise ratios which are caused either by poor slit positioning or by erroneously high magnitudes reported by SExtractor. If the redshift can be measured but no spectral type can be determined, the reasons are usually that the key spectral features fall onto the chip gap or coincide with telluric lines.

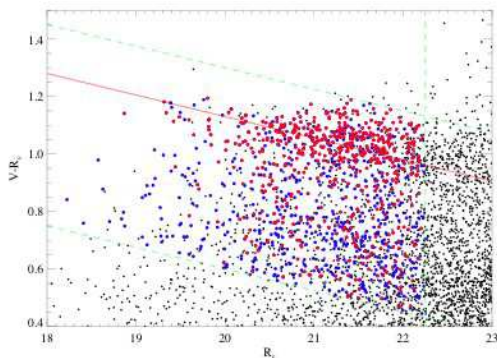


FIG. 4.— Color magnitude diagram for galaxies inside our study region as defined in Fig 2. Blue filled circles mark objects with observed spectra; red filled circles denote spectroscopically confirmed cluster members (cf. Fig. 3). Black dots are all remaining objects in our SExtractor galaxy catalogue. The dashed lines indicate the selection criteria used for our spectroscopic survey. The red sequence marked by the solid line is obtained from a linear fit to the data points redder than $V-R_c \sim 0.9$ and brighter than $R_c \sim 22.5$. [The full resolution figure will be published in ApJ]

³ We include in this statistic a small number of stars which failed to be eliminated by the star-galaxy separation discussed in §3.1

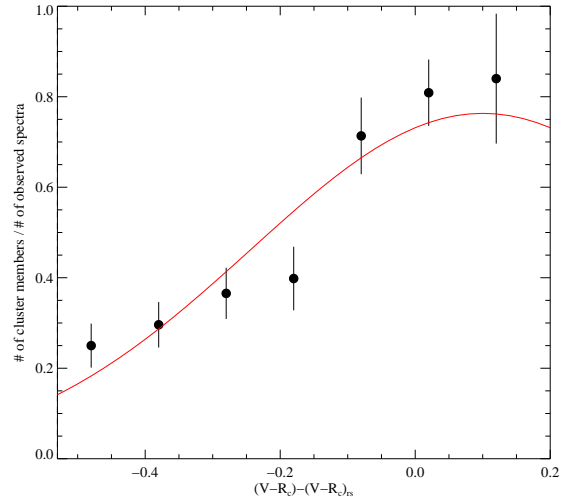


FIG. 5.— The probability of being a cluster member for all galaxies within our study region and brighter than our magnitude cut as estimated by the ratio between the number of cluster members and the number of galaxies with spectroscopic redshift. The x-axis is the relative $V-R_c$ color with respect to the color of the red sequence, which is magnitude dependent (Fig. 4). The fitted function (we use an ad-hoc Gaussian model) allows us to estimate the number of cluster members missed by our survey because of their extremely blue color.

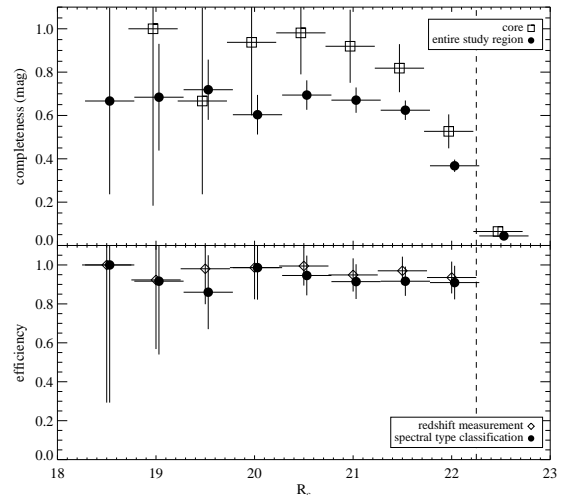


FIG. 6.— Completeness (top) and efficiency (bottom) of our spectroscopic survey as a function of galaxy magnitude. The color criterion of Fig. 4 has been applied. Top: survey completeness for the entire study region (filled symbols) and for Region A (open symbols). Bottom: survey efficiency, i.e. success rate for redshift determination (open symbols) and spectral classification (filled symbols). In both panels, the dashed line indicates the magnitude limit of the spectroscopic sample.

4.2. Equivalent Width Measurement:

In order to allow a comparison of our results with those from previous spectroscopic studies of cluster galaxies we follow the approach of Tran et al. (2003) to measure equivalent widths (EW), i.e. the inverse-variance weighted integration of the flux over a spectral line, using integration windows as defined in Fisher et al. (1998). EW of three spectral features are measured this way: [OII] $\lambda\lambda 3727$, H_δ , and H_γ . For those galaxies with strong emission features but weak or non-detectable continuum, a lower limit to the EW is calculated based on the variance of the spectrum near the spectral feature

in question. An exception is the case of the H_β emission line for which the EW could be underestimated if absorption is present too. We account for this potential bias by subtracting the EW of the H_β absorption as provided by stellar population models (Bruzual & Charlot 2003) fitted to the data from 4060Å to 5360Å (rest frame) using the template-fitting code *pPXF* (Cappellari & Emsellem 2004). We adopt the convention that negative (positive) EW values indicate emission (absorption). Hereafter, we will use the convention that $[OII]$ refers to the EW of [OII] in emission, whereas H_δ and H_γ refer to the EW of the respective lines in absorption. Since we have fitted the emission and absorption components of H_β separately, the EW of H_β in absorption and emission will be specified as $H_{\beta,ab}$ and $H_{\beta,em}$.

4.3. Spectral Type Classification:

We classify cluster galaxies as emission-line galaxies, absorption-line galaxies, and E+A galaxies, following the spirit of the classification used by Tran et al. (2003) with a few modifications⁴. The classification scheme of Tran et al. (2003) only requires the relatively blue features [OII], H_δ , and H_γ , which is convenient for spectroscopic surveys of clusters out to redshift $z \approx 1$ for which redder spectral lines are observationally inaccessible in the optical passband. [OII] emission is an indicator of current activity (be it star formation or the presence of an active nucleus), whereas the two Balmer line features⁵ are indicators of star formation within the last few hundred million years. The Balmer emission lines, however, are more robust diagnostics of star-formation activity (e.g. Moustakas et al. (2006)) than [OII]. Since the latter is easily underestimated because of extinction, the absence of [OII] emission does not necessarily preclude the presence of star formation or other galaxy activity. Although H_α is not accessible to optical surveys for galaxies at $z > 0.5$, the H_β line of most of the galaxies in our target cluster falls within the observable spectral range (although it comes dangerously close to the broad atmospheric H_2O absorption band at 7600Å). We therefore use both $[OII]$ and $H_{\beta,em}$ to define emission-line galaxies, the specific criteria being: $[OII] < -5\text{Å}$ (the same cutoff as Tran et al. (2003)) or $H_{\beta,em} < -5\text{Å}$. Galaxies with $[OII] > -5\text{Å}$ and $H_{\beta,em} > -5\text{Å}$ will be classified as absorption-line galaxies if $\frac{(H_\delta + H_\gamma)}{2} < 4\text{Å}$ (the latter criterion being identical to the one used by Tran et al. (2003)).

As for E+A galaxies, we deviate yet further from Tran et al. (2003) who simply define E+A galaxies to be all galaxies that are neither emission- or absorption-line galaxies. The definition adopted for this work is more conservative in that we require an E+A galaxy to have *no* detectable $[OII]$ or $H_{\beta,em}$ and $\frac{(H_\delta + H_\gamma)}{2} > 6\text{Å}$ (as compared to the cutoff value of 4Å of Tran et al. (2003)). This definition leaves a small fraction of our galaxy sample unclassified, in recognition of the aforementioned gray areas between E+A galaxies and both emission- and absorption-line galaxies.

⁴ Our goal is to classify galaxies according to activity, as reflected in their spectroscopic features. Unfortunately, a universally accepted system for such a classification has yet to be established (see the review in Goto (2006)). This is especially true for E+A galaxies: since the exact locus of the dividing line between E+A galaxies and both emission- and absorption-line galaxies is ill-defined, the final classification in this grey area remains somewhat uncertain.

⁵ It is worth pointing out in this context that historically the classification of E+A galaxies is based on the absorption features H_δ and H_γ , without any attempts at quantifying, or accounting for, emission components in these lines.

The motivation for our choice of more stringent criteria is twofold. As shown by Goto et al. (2003) and Goto (2007), local samples of E+A galaxies compiled without information about H_α may suffer from as much as 52% contamination by H_α emission-line galaxies. Blake et al. (2004), however, found that a linear combination of the strengths of three Balmer absorption lines (H_β , H_δ , and H_γ) can be efficiently used to identify this contaminating population. Following Zabludoff et al. (1996) we thus calculate the average of H_δ , H_γ , and $H_{\beta,ab}$ for all galaxies in our sample that meet the more generous definition of E+A galaxies of Tran et al. (2003), and for which the H_β line is observable. We find that only 45% of them meet the criterion that $\frac{(H_{\beta,ab} + H_\gamma + H_\delta)}{3} > 5.5\text{Å}$ (Blake et al. 2004), implying that more than half of the population thus selected may in fact feature H_α in emission. If, however, we raise the threshold value for $\frac{(H_\gamma + H_\delta)}{2}$ from 4 to 6Å, then 100% of the galaxies thus selected, and for which the H_β line is available, fulfill the criteria of Blake et al. (2004). The second motivation for our more stringent definition of E+A galaxies is that the detection of [OII] in a galaxy is not an unambiguous sign of star formation but could also be indicative of non-stellar radiation. Indeed, Yan et al. (2006) find that a large fraction of post-starburst galaxies may be misidentified as undergoing current star formation, although the [OII] emission actually originates from AGN. Since our project has currently no means of efficiently distinguishing between star-bursting galaxies and post-starburst galaxies containing AGN, and since the compilation of a statistically complete sample of post-starburst galaxies is not the main goal of this work, we exclude from our E+A sample all galaxies featuring *any* [OII] emission, in order to keep the resulting sample as clean as possible and avoid complications caused by the presence of AGN for the interpretation of the mechanisms responsible for the termination of star formation activity. Although the sample of E+A galaxies selected by our more conservative criteria thus misses a possibly sizeable and interesting fraction of the entire post-starburst population as suggested in Yan et al. (2006), it is better suited to study the interactions between galaxies and the intra-cluster medium, and it is also less contaminated by weakly star-forming galaxies.

Following Dressler et al. (1999), we can classify the emission-line galaxies further into e(a), e(b), and e(c) subtypes based on the strength of the H_δ absorption and $[OII]$ emission lines. Both of these features are indicative of starbursts within a few million years to one billion years before the time of observation. Specifically, e(a) galaxies are defined as systems with $H_\delta > 4\text{Å}$ and $-40\text{Å} < [OII] < -5\text{Å}$, whereas e(b) galaxies feature $[OII] < -40\text{Å}$, regardless of H_δ ; the spectral evidence of young and massive stars in either of these subtypes suggests recent starbursts. All other emission-line galaxies, i.e. systems lacking signs of explosive star formation in the recent past are classified as e(c). The difference between e(b), e(a), and E+A galaxies is thus the decreasing strength of the [OII] emission line. The absence of [OII] in E+A galaxies suggests that the star formation activity is halted, whereas, at the opposite extreme, strong [OII] emission makes the e(b) sub-type promising candidates of starburst galaxies. The, in terms of [OII] strength, intermediate e(a) galaxies, on the other hand, are not easily placed in this sequence since, as mentioned before, the strength of [OII] emission is highly sensitive to

dust extinction. Poggianti & Wu (2000), for instance, find about half of a sample of very luminous infrared galaxies [$\log(L_{IR}/L_{\odot}) > 11.5$] to exhibit e(a) spectra. The distinction between these three populations is thus ambiguous; some of the E+A galaxies may actually be e(a) galaxies whose [OII] emission is completely extinguished by dust. Conversely, some of the e(a) galaxies could in fact be post-starburst galaxies with some residual star formation. In spite of these ambiguities, we emphasize that e(a) and E+A galaxies are in general distinct populations, which is – as we shall demonstrate – reflected in their different distribution within the cluster environment. The relevance of e(a) and e(b) galaxies in the context of this study is the potential for both galaxy types to trace the E+A progenitor population.

For clarity, the definition of the spectral types is summarized in Table 2. The number of galaxies of each type is given in Table 3. Note that, because of our conservative definition of E+A galaxies, about 8% of all cluster members with spectroscopic information are missing in Table 3 as well as in the analysis that follows. They are the population with weak [OII], weak H_{β} , and Balmer absorption lines whose strength falls between the absorption-line and E+A criteria ($4\text{\AA} < \frac{(H_{\delta} + H_{\gamma})}{2} < 6\text{\AA}$). They are probably a mixture of dusty star-forming galaxies and post-star-forming galaxies. In Tran et al. (2003) and Tran et al. (2004), galaxies of this type are also classified as E+A galaxies.

5. RESULT:

5.1. Photometric Redshift

From our photometry in the u^* , B, V, R_c , I_c , and z' bands, photometric redshifts are derived for galaxies with $R_c < 24.0$ ($\sim M^* + 4$ at $z=0.55$) using the adaptive SED-fitting code *Le Phare* (Arnouts et al. 1999; Ilbert et al. 2006). *Le Phare* employs χ^2 optimization, comparing the observed magnitudes with those predicted from an SED library. An adaptive method is applied to adjust the photometric zero-points for all passbands by using the sample of spectroscopic redshifts as a training set⁶. No Bayesian prior for the galaxy redshift distribution is assumed. We use the library of empirical templates of Ilbert et al. (2006) and the Calzetti extinction law (Calzetti 2001) for reddening corrections applied to templates later than Sbc. The training set is obtained from the spectroscopic redshift database by selecting all galaxies with an R_c -band magnitude brighter than 21.5 and a minimal separation from the closest SExtractor-detected neighbor of $3.5''$ to avoid photometric errors from close pairs or blended sources. The resulting training set comprises 273 galaxies at redshifts ranging from 0.15 to 0.9. The comparison of spectroscopic and photometric redshifts is shown in Fig. 8. The statistical error of the photometric redshifts, as derived from the Gaussian distribution of the residuals shown in the insert of Fig. 8, is found to be $\Delta z = 0.024$.

The main purpose of the photometric redshift catalogue is to allow us to estimate the local projected galaxy density with better statistics than would be feasible from the spectroscopic data set alone. On the basis of photometric redshifts, we define cluster members to be the galaxies with $|z_{ph} - z_{cl}| < \sigma_{ph-z}$, where $\sigma_{ph-z} = (1 + z_{cl})\Delta z$. Note that this redshift cut ($\pm\sigma_{ph-z} = \pm 0.036$) is much more generous than that used before for the spectroscopic redshifts ($\pm 3\sigma = \pm 0.022$);

⁶ The resulting correction of typically 0.05 mag is consistent with the statistical and systematic uncertainty of our photometric calibration.

the chosen cutoff value represents a good compromise between completeness and contamination. The resulting catalogue of “photometric” cluster members includes 2218 galaxies and allows us to estimate the local galaxy density in the entire Suprime-Cam field of view. The much higher accuracy of our spectroscopic redshifts, on the other hand, provide us with an opportunity to study the dynamical structure of the cluster-filament system in detail.

Using the photometrically selected set of cluster members, we map the surface density of cluster galaxies. A smoothed version of this distribution (shown in Fig. 2) is obtained with the adaptive-smoothing algorithm *asmooth* (Ebeling et al. 2006) which preserves the signal-to-noise ratio of all significant features on all scales. The comparison of the result with the maps derived by Ebeling et al. (2004) and Kartaltepe et al. (2008) using only galaxies on the cluster red sequence proves instructive in as much as it highlights the dominance of blue galaxies in low-density, filamentary environments. We show in Fig. 7, side by side, the galaxy surface density maps obtained by us using photometric redshifts as described above, and the equivalent map from Kartaltepe et al. (2008) which is based entirely on galaxies with $V-R_c$ colors consistent with the cluster red sequence. Note the dramatic difference in the relative prominence of the main cluster and the filament.

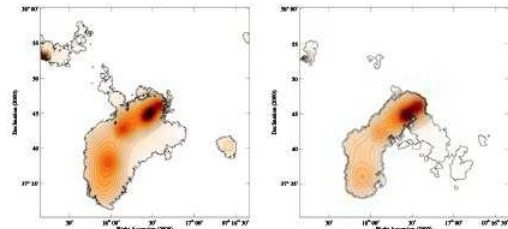


FIG. 7.— Surface density of cluster members using either photometric redshifts (top) or selection by red-sequence color (bottom) (Kartaltepe et al. 2008). The contour levels are given by $1.2^n \Sigma_{bkg}$, where Σ_{bkg} is the background surface density of each plot. The bold, ragged contour marks the boundary of regions outside of which the significance of any structure in these adaptively smoothed images falls below the 3σ confidence level. [The full resolution figure will be published in ApJ]

In order to allow a direct comparison with the results from earlier work on the impact of cluster environment on galaxy activity (Kodama et al. 2001; Balogh et al. 2004; Sato & Martin 2006), we also calculate for all “photometric” cluster members the projected local density Σ_{10} , defined as the galaxy number density within a circle whose radius is given by the separation to the 10^{th} closest neighbor. The resulting values of Σ_{10} are consistent with the surface density distribution shown in the top panel of Fig. 7.

5.2. Broad-Band Colors of Cluster Members of Different Spectral Types

The comparison of Fig. 4 with the color-magnitude diagram for different spectral types of galaxies (left panel of Fig. 9) illustrates the potential bias caused by the blue color cut discussed in §4.1. Not surprisingly, all of the bluest cluster members found in our study are emission-line galaxies, the fraction of which is thus likely to be underestimated. This is particularly true for the e(b) subtype which we find to be heavily concentrated at the blue, faint end of our selection in color-magnitude space. If all cluster members bluer than our color

TABLE 2
DEFINITION OF SPECTRAL TYPES

Type	Criteria
Emission-line	$[OII] < -5\text{\AA}$ or $H_{\beta,em} < -5\text{\AA}$
Absorption-line	$[OII] > -5\text{\AA}$ $H_{\beta,em} > -5\text{\AA}$ and $\frac{(H_{\delta}+H_{\gamma})}{2} < 4\text{\AA}$
E+A	no detection of $[OII]$ and $H_{\beta,em}$, and $\frac{(H_{\delta}+H_{\gamma})}{2} > 6\text{\AA}$
e(a)	Emission-line galaxies with $H_{\delta} > 4\text{\AA}$ and $-40\text{\AA} < [OII] < -5\text{\AA}$
e(b)	Emission-line galaxies with $[OII] < -40\text{\AA}$
e(c)	Emission-line galaxies with $H_{\delta} < 4\text{\AA}$ and $-40\text{\AA} < [OII] < -5\text{\AA}$

TABLE 3
SPECTRAL TYPES SUMMARY

Type	All	cluster members
all spectra ^a	1368	...
sample spectra	1147	...
redshift measurements	1103	563
spectra with spectral diagnostics	1023	530
Emission-line galaxies	507	203
Absorption-line galaxies	426	260
E+A galaxies	21	17
Unclassified	69	50
e(a)	76	42
e(b)	66	27
e(c)	365	134

^a No magnitude or color cuts are applied. Spectra obtained serendipitously are included.

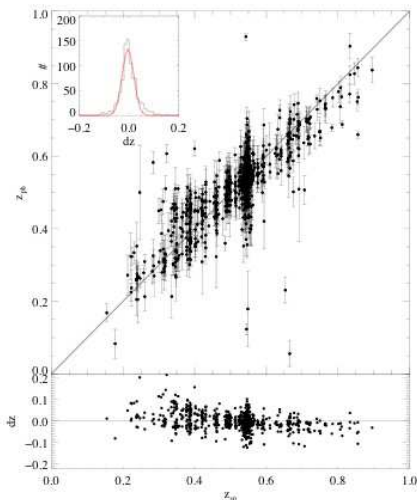


FIG. 8.— Photometric versus spectroscopic redshifts for galaxies in the field of MACSJ0717.5+3745; we only show galaxies from our *Le Phare* training set (see text for details). The lower panel shows the residuals dz as a function of the spectroscopic redshift, while the insert in the top left corner shows the histogram of the residuals as well as a Gaussian model used to estimate their standard deviation Δz . [The full resolution figure will be published in ApJ]

cut are in fact e(b) galaxies – clearly the worst-case scenario –, the number of e(b) galaxies in MACSJ0717.5+3745 could be underestimated by as much as $\sim 30\%$. We shall keep this in mind when, later, discussing the fraction of e(b), e(a), and emission-line galaxies in general. Note, however, that the E+A and absorption-line galaxies lie well away from the color cut, so that their numbers can be expected to be unaffected by color-dependent incompleteness.

Figure 9 compares the magnitude and color distributions of cluster members of different spectral type. As has been noted

before by other authors, for example Dressler & Gunn (1983), Tran et al. (2003), and Tran et al. (2007), E+A galaxies are found to exhibit broad-band colors that are intermediate between those of absorption- and emission-line galaxies, as is to be expected from their spectral definition as a composite of old and new stellar populations. Differences between the various spectroscopic types can be characterized by measuring the mean and scatter of the relative $V-R_c$ color of a given galaxy class with respect to the red sequence (Table 4). The mean relative color of zero found for absorption-line galaxies confirms our linear fit to the cluster red sequence calculated without selection of any specific spectroscopic types (Fig. 4). The small scatter in the relative $V-R_c$ color of absorption-line galaxies is consistent with the result of, e.g., Blakeslee et al. (2006) and Tran et al. (2007) that early-type cluster members are formed at $z \sim 2$. The mean relative colors of the other spectroscopically defined galaxy types discussed in this study are, in order of increasing blueward distance from the red sequence, E+A galaxies, e(a), and e(b) galaxies, a ranking consistent with the hypothesis that E+A galaxies represent an intermediate stage in the evolutionary sequence from active emission-line galaxies to passively evolving early-type galaxies. Interestingly, this scenario is also supported by the different scatter around the mean relative color for the different populations: the color scatter of the E+A galaxies is significantly smaller than the one of e(a) and e(b) galaxies, their potential precursors (Poggianti et al. 1999), but still larger than the one of the evolved population of absorption-line galaxies forming the cluster red sequence. Although their spectral properties imply that E+A galaxies evolved from the e(a) and/or e(b) population less than one billion years ago, their color characteristics have thus already become remarkably similar to those of absorption-line galaxies.

Another interesting fact that emerges from Fig. 9 relates to the mean color of e(b) galaxies. Their locus at the extreme blue end of the distribution shown in the left bottom panel of Fig. 9 is not solely the result of the strong $[OII]$ emission to which they owe their definition. Since $[OII]$ falls into the V band at $z = 0.55$, the fact that the majority of the e(b) galaxies found in our study also exhibits very blue U-V colors (right bottom panel of Fig. 9) indicates significant continuum emission in the UV rest frame. Follow-up observations are needed of the few e(b) galaxies that are found to be unusually red to establish whether nuclear activity is responsible for the strong $[OII]$ emission observed.

5.3. Dynamical Scales

A fundamental problem of many forms of dynamical analysis is the inherent assumption of virial equilibrium. Models appropriate for the description of clusters in the process of active assembly, such as MACSJ0717.5+3745 or – albeit to a lesser degree – MS0451.6-0305 (Moran et al. 2007), would

TABLE 4
RELATIVE COLOR STATISTICS OF SPECTROSCOPIC TYPES

	mean ^a	scale ^a
Absorption-line galaxies	$0.00^{+0.005}_{-0.004}$	$0.0068^{+0.0004}_{-0.0004}$
E+A galaxies	$-0.05^{+0.03}_{-0.03}$	$0.08^{+0.01}_{-0.03}$
Emission-line galaxies ^b	$-0.26^{+0.01}_{-0.02}$	$0.176^{+0.009}_{-0.006}$
e(a) galaxies ^b	$-0.30^{+0.02}_{-0.03}$	$0.12^{+0.01}_{-0.02}$
e(b) galaxies ^b	$-0.42^{+0.04}_{-0.04}$	$0.18^{+0.02}_{-0.06}$
e(c) galaxies ^b	$-0.23^{+0.02}_{-0.02}$	$0.175^{+0.01}_{-0.009}$

^a Mean and scale are calculated using the biweight estimator in Beers et al. (1990)

^b Because of the blue color cut mentioned in §4.1, the mean and scattering of the emission-line galaxies and the subtypes, in particular the e(b) galaxies, may be biased.

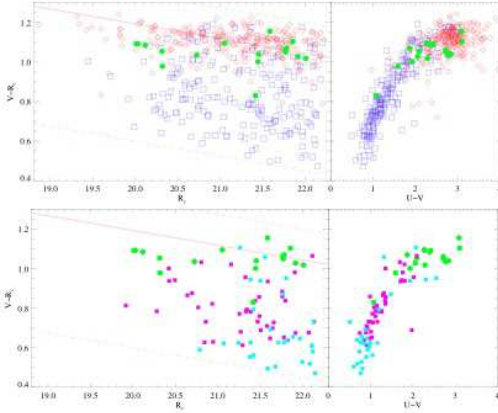


FIG. 9.— Top: (left) Color-magnitude diagram for galaxies of different spectral type. Open red diamonds mark absorption-line galaxies, open blue squares emission-line galaxies, and filled green circles E+A galaxies. The dashed lines are the color and magnitude cuts from Fig. 4. (right) U-V vs. V-R_c of galaxies of different spectral type. Bottom: same as top panel, but showing E+A galaxies in comparison with their hypothesized progenitor population, e(a) and e(b) galaxies (magenta and cyan symbols respectively). [The full resolution figure will be published in ApJ]

TABLE 5
CLUSTER PROPERTY

	value	unit
f_x ^a	2.74 ± 0.03	10^{-12} ergs s ⁻¹ cm ⁻²
L_x ^a	24.6 ± 0.3	10^{44} ergs s ⁻¹
kT ^a	11.6 ± 0.5	keV
β	1.1 ± 0.1	
ρ_0	1.71 ± 0.05	$10^{14} M_\odot \text{Mpc}^{-3}$
r_c	92 ± 6	arcsec
z_{cl} ^b	0.5446 ± 0.0005	
σ ^b	1612 ± 70	km s ⁻¹
$R_{vir,gal}$ ^c	3.0 ± 0.2	Mpc
$R_{vir,x-ray}$ ^c	2.9 ± 0.1	Mpc
M_x ^c	28 ± 5	$10^{14} M_\odot$
R_{rs}	1.9	Mpc

^a Ebeling et al. (2007)

^b The values for the mean redshift z_{cl} and velocity dispersion σ are calculated iteratively using the redshifts of cluster members within the virial radius (2.9 Mpc) and thus differ slightly from the values published by Ebeling et al. (2007) where a radius of 1 Mpc was used.

^c The uncertainty is estimated by error propagation.

have to take into account the effects of mergers and complex substructure on a wide range of scales. With the exception of the simplest cases this is infeasible, in part owing to our in-

sufficient knowledge of the true three-dimensional geometry of the system. With this caveat in mind, we note that the simplistic dynamical scales derived in this section should only be considered crude estimates.

The most relevant dynamical scales for this work are the virial radius R_{vir} and the ram-pressure stripping radius R_{rs} . To obtain estimates of these quantities, we need a description of the cluster's gas density profile as well as a global X-ray temperature. The former is obtained by fitting a β -model (Cavaliere & Fusco-Femiano 1976)

$$\rho_{gas} = \rho_0 \left[1 + \left(\frac{r}{r_c} \right)^2 \right]^{-\frac{3}{2}\beta} \quad (1)$$

to the observed X-ray surface brightness. Specifically, the center of the X-ray emission is determined by fitting a two-dimensional elliptical β -model to the exposure-weighted image after point sources have been removed. The radial profile is then extracted using this center position. The subsequent fit of a one-dimensional β -model is limited to radii larger than $11''$ (70 kpc) to minimize the impact of the complex merging features in the heavily disturbed cluster core. A global X-ray temperature is measured by extracting the X-ray spectrum from $r = 70$ kpc to $r = 0.94$ Mpc (r_{1000}) and using *Sherpa* to fit a MEKAL plasma model (Mewe et al. 1985) with the absorption term frozen at the Galactic value. From the X-ray temperature and the β -model profile, we estimate the virial radius R_{vir} using the formula of Arnaud et al. (2002)

$$R_{vir} = 3.80 \beta_T^{1/2} \Delta_z^{-1/2} (1+z)^{-3/2} \times \left(\frac{kT}{10\text{keV}} \right)^{1/2} h_{50}^{-1} \text{Mpc}$$

with

$$\Delta_z = (200\Omega_0)/(18\pi^2\Omega_z).$$

Here β_T is the normalization of the virial relation, i.e., $GM_v/(2R_{vir}) = \beta_T kT$. The virial radius thus derived is about 2.9 Mpc, which is consistent with the virial radius (3 Mpc) estimated from the velocity dispersion using the relation (Gunn & Gott 1972)

$$R_{vir} = 1.7h^{-1}\text{Mpc} \frac{\sigma}{1000 \text{ km s}^{-1}} [\Omega_m(1+z)^3 + \Omega_\Lambda]^{-0.5}.$$

The ram-pressure stripping radius is estimated by equating the gas pressure required to strip a Milky-Way-like galaxy from all its gas to the gas density obtained previously in our X-ray analysis (Eqn. 1). The former can be obtained from the stripping requirement (Gunn & Gott 1972; Treu et al. 2003)

$$\rho_{gas} v_i^2 > 2.1 \cdot 10^{-12} \text{Nm}^{-2} \left(\frac{v_{rot}}{220 \text{ km s}^{-1}} \right)^2 \left(\frac{r_h}{10 \text{ kpc}} \right)^{-1} \times \left(\frac{\Sigma_{HI}}{8 \cdot 10^{20} m_H \text{ cm}^{-2}} \right)$$

Here v_i is the velocity of the infalling galaxy which, in all other respects (rotation velocity v_{rot} , scale length r_h , and HI surface density Σ_{HI}), is assumed to be similar to the Milky Way, as indicated by the units used above. The infall velocity v_i is estimated as

$$v_i(r) = \sqrt{\frac{2GM_x}{r} - \frac{GM_x}{R_{vir}}},$$

where M_x is the total mass within R_{vir} derived from the X-ray properties of the cluster (see, e.g., Maughan et al. (2003)). A summary of the results as well as of related X-ray cluster properties is given in Table 5.

Additional dynamical scales, that are of less interest to us here, can be computed to assess the efficiency of tidally triggered star formation, tidal stripping, starvation, harassment, and galaxy mergers. As discussed by Treu et al. (2003), the first two effects are only important within a few hundred kpc of the cluster core and are thus difficult to study statistically for any single cluster. In addition, the complex X-ray morphology in the core of MACSJ0717.5+3745 makes this system particularly ill-suited for quantitative modeling. Starvation and harassment, on the other hand, are efficient at larger radii, with the starvation radius being equivalent to the virial radius (Balogh et al. 2000), and harassment being almost independent of cluster-centric distance (Moore et al. 1996, 1998). Since probably all cluster galaxies under study here are thus subject to harassment, it would not be easy to isolate the impact of this particular effect. The last mechanism, galaxy merging, is largely irrelevant in the densest parts of the cluster environment, owing to the large velocity dispersion, but peaks near the virial radius (see e.g. (Ghigna et al. 1998)).

5.4. Redshift Distribution of Cluster Members

The dynamical scales derived in the previous section refer to the primary cluster, but exclude the filament. As a first look into the properties of the large-scale structure observed, all the way from the cluster core to the extended peak in the galaxy density in Region B, we show in Fig. 10 the distribution of galaxy redshifts projected onto a line starting northwest of the cluster center and ending southeast of the filament, as indicated in Fig. 2. We find the average redshift of the galaxies in Region B, $\bar{z}_B = 0.5468 \pm 0.0004$, to be significantly higher than that of the galaxies around the main cluster, $\bar{z}_A = 0.544 \pm 0.0006$. The velocity difference between these two regions is thus 630 km/s. In addition, the velocity dispersion of the galaxies in Region B is $\sigma_{z,B} = (1050 \pm 65)$ km/s, significantly less than the value of $\sigma_{z,A} = (1630^{+75}_{-93})$ km/s found in Region A. Although the Chandra ACIS-I image of MACSJ0717.5+3745 covers a fair fraction of Region B, it just misses the galaxy density peak at its center. Since, in addition, the exposure of this observation is only 60 ks, we are currently unable to obtain an estimate of the gas temperature and mass in Region B. Deriving a mass estimate from $\sigma_{z,B}$ is not meaningful because of the clearly unvirialized nature of this structure.

5.5. Spatial Distribution of Cluster Members

We show in Fig. 11 the distribution of different galaxy types as a function of (radial) distance to the cluster center. The fraction of absorption-line galaxies drops from $\sim 80\%$ in the cluster core to $\sim 30\%$ at the virial radius, where the fraction of emission-line galaxies shows the opposite behavior, increasing from about 5% at the cluster center to almost 70% at the virial radius. Beyond 3.5 Mpc, however, both trends are reversed as we approach the galaxy density peak of Region B at 4.5 Mpc. At the largest radii probed by our study, the ratio of the numbers of absorption- and emission-line galaxies begins to approach the field value. An interpretation of our data in the context of the well known morphology-density relation (Dressler 1980) will be given in the next section.

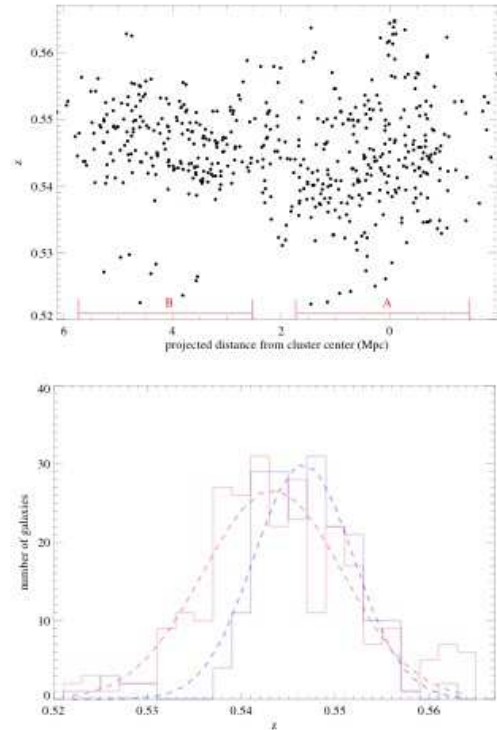


FIG. 10.— Top: redshift distribution of cluster members as a function of their projected distance from the cluster center, measured along the line shown in Fig. 2. Bottom: redshift histogram for galaxies in the two regions A and B of Fig. 2; the red lines refer to Region A (cluster center), the blue lines to Region B (filament). [The full resolution figure will be published in ApJ]

Interestingly, the distribution of E+A galaxies follows neither of the above trends. Rather, almost all E+A galaxies (16 out of 17) are found to reside in Region A. No E+A galaxy is detected at cluster-centric distances exceeding 2 Mpc, with the sole exception of a single specimen near the southern edge of Region B. Remarkably, the radial locus of the abrupt decline in the number of E+A galaxies thus coincides almost perfectly with the ram-pressure stripping radius, $R_{rs} = 1.9$ Mpc.

The spatial distribution of starburst galaxies is very different again: the distribution of both e(a) and e(b) galaxies follows, qualitatively, the distribution of their parent type, emission-line galaxies in general. Comparing the e(a) and e(b) distributions, the fraction of e(b) galaxies appears to show a more gradual and monotonic rise with cluster-centric distance than that of e(a) galaxies. The difference between the e(a) and e(b) distributions is, however, not significant: a Kolmogorov-Smirnov test finds the probability of them being drawn from the same parent distribution to be 0.69. We note though, that the aforementioned incompleteness of up to 30% in our e(b) sample would likely increase the fraction of e(b) galaxies at all cluster-centric radii.

Although more difficult to interpret quantitatively, the two-dimensional spatial distribution of galaxies of different spectral types provides additional insight. To facilitate a visual analysis, we show, in Fig. 12, the respective distributions separately for emission-line galaxies, absorption-line galaxies, and – in a third panel – E+A, e(a), and e(b) galaxies. The contours of the projected galaxy density of Fig. 7 (top panel) are overlaid. We compare the distributions shown in these three panels in the following.

The absorption-line galaxies are strongly concentrated in

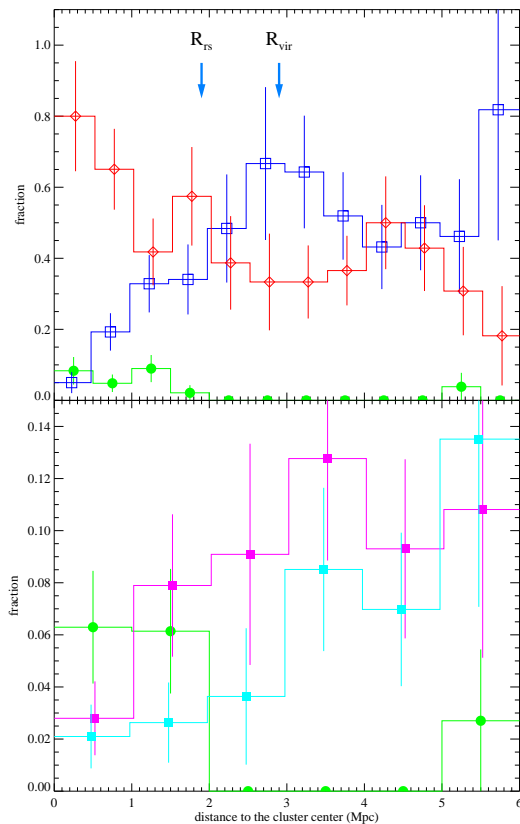


FIG. 11.— Distribution of galaxies of different spectral type with cluster-centric distance. The symbols the same as in Fig. 9. In each bin the fraction is calculated by dividing the number of member galaxies of a given spectral type by the total number of member galaxies observed spectroscopically. The plotted error bars assume Poisson statistics. Some symbols are shifted slightly by ± 0.02 Mpc for clarity.

the double core of MACSJ0717.5+3745 proper, a region which is almost entirely devoid of emission-line galaxies. High concentrations of absorption-line galaxies are also found at the locations of two galaxy groups embedded in the filament, both of which are also detected in X-rays (Fig. 1). The string of three high-density regions near the nominal cluster center thus causes an excess of absorption-line galaxies in Region A, which extends linearly over almost 3 Mpc northwest to southeast of the cluster core. By contrast, the observed overdensity of cluster members in Region B has a much less pronounced effect on the distribution of absorption- and emission-line galaxies: overall, both galaxy types exhibit similar concentrations. Interestingly, absorption-line galaxies in this region are, however, found preferentially south of the center of Region B, whereas emission-line galaxies dominate the northern part of this area, roughly 0.5 Mpc away in projection. It is this large-scale segregation between absorption- and emission-line galaxies that is responsible for the shift of the overall distribution of cluster members in Region B shown in the top and center panel of Fig. 7; the apparent, not well defined center of this region is inhabited by a concentration of e(a) and e(b) galaxies (bottom panel of Fig. 7). Relating these observations to the true three-dimensional distribution of galaxy types in Region B is, however, greatly complicated by both projection effects and the likely presence of significant peculiar velocities (Barrett 2005). Looking at yet larger scales, it is clear from Fig. 12 that the distribution of emission-line galaxies is vastly more extended over our study region

than is the distribution of absorption-line galaxies. The lack of pronounced overdensities in the distribution of emission-line galaxies suggests strongly that a significant fraction of emission-line galaxies observed apparently near high-density regions of the MACSJ0717.5+3745 system are in fact projected there from much larger distances along the line of sight. This point is worth keeping in mind for the interpretation of the true spatial distribution of all types of emission-line galaxies.

E+A galaxies, finally, are found to be distributed almost evenly within the ram-pressure stripping radius R_{rs} ; we again note, however, the likely presence of projection effects. Since the small number of E+A galaxies in our sample does not allow us to derive a deprojected radial density profile, we can, at present, not distinguish between a spatial model in which E+A galaxies inhabit a shell around the cluster core, and one in which their distribution increases toward the cluster core as is expected for the absorption-line galaxies. Although a comparison of the respective projected radial distributions of E+A and absorption-line galaxies suggests the former, a Kolmogorov-Smirnov test finds them to be consistent with each other at the 1σ confidence level. From our study of this cluster alone we are thus unable to address the issue of whether E+A galaxies avoid the very cores of galaxy clusters as has been suggested by other authors (Tran et al. 2003; Dressler et al. 1999).

5.6. Projected Density Distribution of Cluster Galaxies

One of the most important parameters for studies of galaxy evolution is the density of the local environment. In Fig. 13 we plot the fraction of galaxies of different types as a function of the projected local galaxy density, Σ_{10} , as estimated from the sample of photometrically selected cluster members (i.e., $z_{ph} = 0.507$ to 0.580). The observed monotonic rise and fall of the fractions of emission- and absorption-line galaxies (top panel) with decreasing galaxy density, Σ_{10} , confirms our interpretation of the trends already seen in Fig. 11 and suggests strongly that the projected density is a more fundamental physical parameter for the distribution of the emission- and absorption-line galaxies than the distance to the cluster center. This result is consistent with the relation between star-formation rate and local density, as well as with the morphology-density relation, from studies of other clusters at intermediate redshift (Dressler 1980; Poggianti et al. 1999; Kodama et al. 2001). Note, however, how the fraction of either galaxy type is almost insensitive to the density of the environment until the latter reaches a value typical of galaxy groups ($\sim 20 \text{ Mpc}^{-2}$), at which point the divide between absorption- and emission-line galaxies begins to open up dramatically (Kodama et al. 2001).

The bottom panel of Fig. 13 emphasizes the stark contrast between the environmental dependence of E+A galaxies and that of e(a) and e(b) galaxies. The latter two galaxy types appear to, qualitatively, follow the trend already seen for emission-line galaxies in general (which is not all that surprising given that the e(a) and e(b) classification denotes subtypes of emission-line galaxies), but with a possibly higher sensitivity to local density already at values well below those characteristic of galaxy groups. E+A galaxies, on the other hand, appear to follow the opposite trend of favoring environments of intermediate to high density.

The histogram of the Σ_{10} values observed in Region A and Region B shown in Fig. 14 illustrates that the range of projected local galaxy densities in Region B overlaps signif-

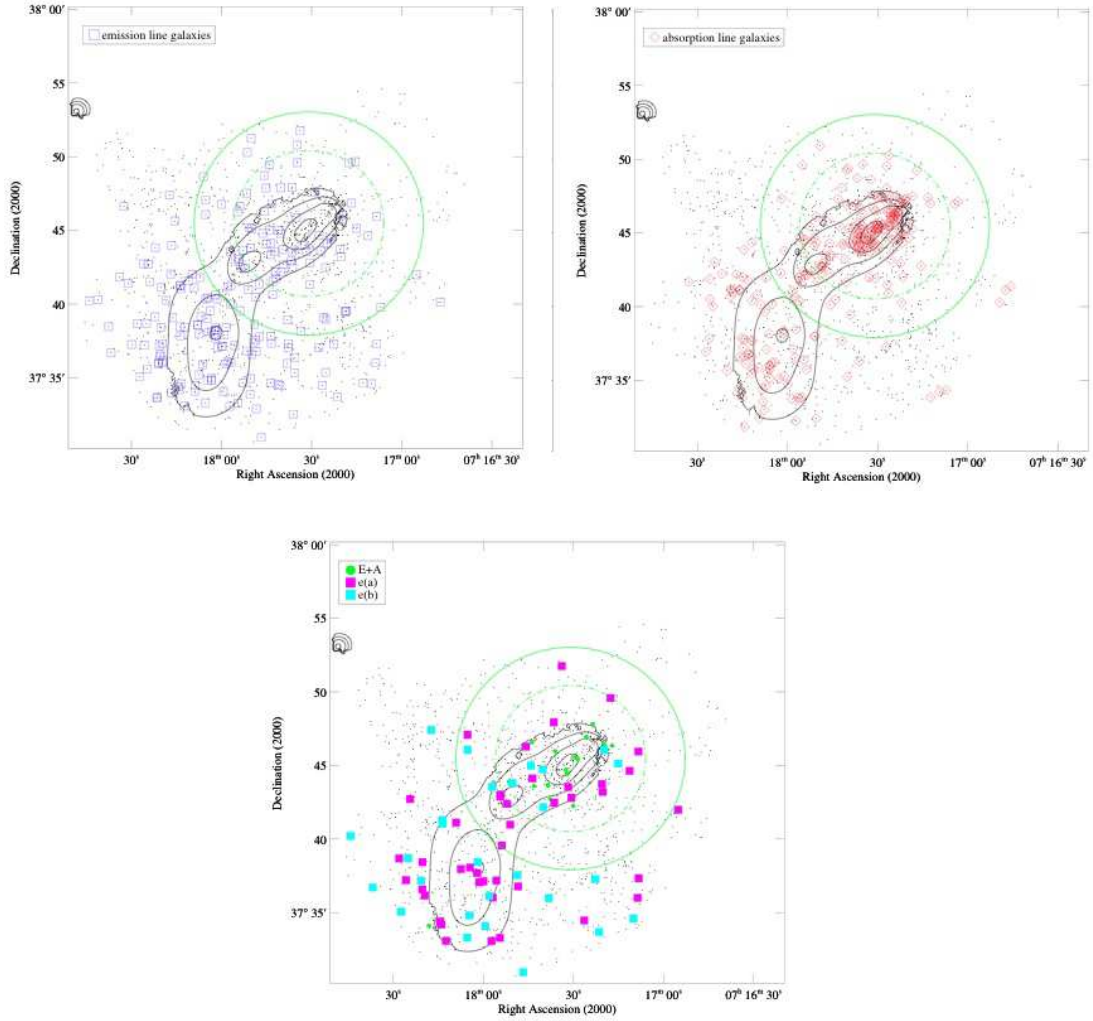


FIG. 12.— Projected spatial distribution of different galaxy types in the MACSJ0717.5+3745 system. Symbols are as in Fig. 9, with the addition of small black dots which mark the locations of all galaxies within our study region that have been observed spectroscopically. Also shown are the galaxy-density contours from Fig. 2. The green circles have radii of R_{vir} (dashed) and R_{rs} (solid), respectively, as estimated in §3.3 [The full resolution figure will be published in ApJ]

icantly with the one encountered in the primary cluster region. Indeed, both emission- and absorption-line galaxies show the same trends in either region (Figs. 11,13): their fractions are mainly a function of Σ_{10} . This is not true for E+A galaxies: although the majority of E+A galaxies found in MACSJ0717.5+3745 are associated with Σ_{10} values that are most commonly encountered in Region B, only one out of our 17 E+A galaxies is in fact detected there. If density were the determining factor in the creation of E+A galaxies, their distribution with Σ_{10} in Region A would lead to a prediction of 9 E+A galaxies in Region B – a number that is inconsistent with the observed count of one at the 3σ significance level. We conclude that, at least for the system under investigation here, the physical mechanism responsible for the termination of star formation in this galaxy type must be a different one.

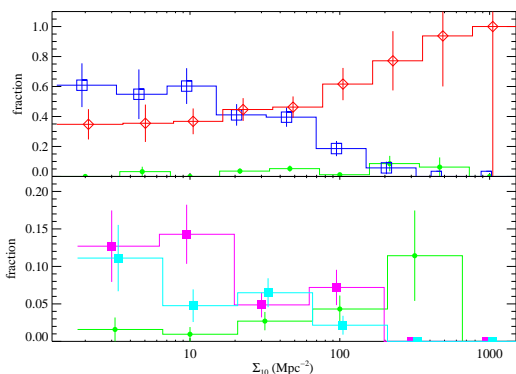


FIG. 13.— Fraction of galaxies of different spectral types as a function of projected local density. Symbols are as in Fig. 12. Error bars assume Poisson statistics. The symbols for E+A galaxies and absorption-line galaxies are slightly shifted horizontally for clarity.

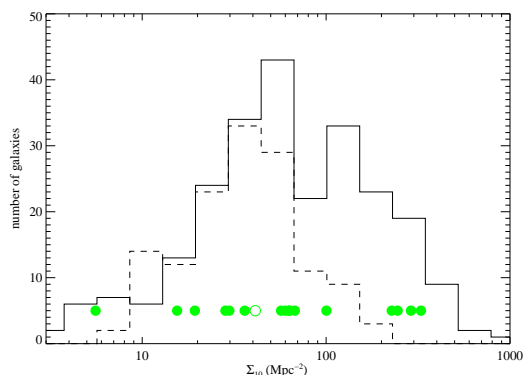


FIG. 14.— Histogram of projected local galaxy densities for Region A (solid line) and Region B (dashed line). See Fig. 2 for a definition of these regions. The filled (open) green circles mark the densities at which we detect E+A galaxies within Region A (B).

6. DISCUSSION

The arguably most interesting result of our spectral analysis of the galaxy population of the cluster/filament system MACSJ0717.5+3745 is the spatial distribution of E+A galaxies, which may provide important clues about the physical mechanism triggering the E+A transition phase between actively star forming and passively evolving galaxies. Three aspects need to be considered in this context: what is the origin

of the galaxies that evolve into E+A galaxies, what are the mechanisms that trigger the starburst, and what are the mechanism(s) responsible for terminating it?

6.1. E+A Progenitors

A first clue about the origin of the E+A galaxies in MACSJ0717.5+3745 can be obtained from their spatial distribution. If the galaxies that develop the E+A spectral characteristics originated from the large-scale filament or the galaxy groups embedded therein, one would expect E+A galaxies to be found preferentially near the filament-cluster interface. According to Fig. 12 this is not the case. Although the spatial distribution of E+A galaxies exhibits a slight elongation in the direction of the (projected) direction of infall along the filament, their location with respect to the cluster core is consistent with a roughly spherical distribution which, in turn, suggests an isotropic distribution of the progenitor population.

A different approach would be to attempt to directly identify the most likely progenitors. The strong $H\delta$ absorption in the spectra of E+A galaxies indicates that not only the starburst stopped both abruptly and recently (within a few hundred millions years), but also that a very significant population of young stars was thus generated (e.g. Barger et al. (1996), and the review in Poggianti et al. (2004)). This is particularly true for this study since we have intentionally selected the E+A galaxies with extreme Balmer absorption features. Galaxies currently undergoing strong star formation i.e., the e(a) and e(b) subtypes of emission-line galaxies, are thus natural candidates for the role of progenitors of E+A galaxies, and should, to some extent, trace the spatial distribution of the progenitor population. Examining, again, Fig. 12 we see that both e(a) and e(b) galaxies show a rather flat distribution which, however, prefers the general direction of the filament and is, globally, distinctly un-isotropic with respect to the cluster core. Although the distribution of e(a) and e(b) galaxies thus does not rule out the hypothesis that the filament represents an important reservoir from which E+A galaxies originate, the combined evidence appears to favor a picture in which E+A galaxies evolve from a population of galaxies residing predominantly in a halo surrounding the entire cluster+filament complex. The characteristic density of this typical e(a)/e(b) environment is higher than that of the infall region but lower than the one found in galaxy groups — as a result, these potential E+A progenitors are missing from the denser regions of our study area as well as from the field.

Results from our complete survey of the galaxy population of the most distant MACS clusters should allow us to address these issues with a much larger degree of certainty.

6.2. Source of Starburst Galaxies

The next question is how the starbursts are triggered in cluster galaxies. The spatially fairly even distribution of e(a) and e(b) galaxies Fig. 12, which nonetheless shows a preference for the general area of the filament, represents evidence that starbursts are triggered in regions well outside the cluster, and in fact well outside the central regions of the filament too. The densities typical of the environment in which e(a) and e(b) galaxies predominantly reside can be estimated from both the spatial distribution in the filament region (Fig. 12) and our direct measure of the projected galaxy density (Fig. 13). Taking into account the certainty of projection effects we arrive at §5.5. This result that star formation is triggered at radii approaching the virial radius and environmental densities well

below that of galaxy groups is qualitatively consistent with the findings of Kodama et al. (2001) and Marcillac et al. (2007).

6.3. Star Formation Termination

Although it is generally accepted that environmental effects other than galaxy mergers are important to quench star formation in E+A galaxies in clusters (Tran et al. (2003) and references therein), there has, so far, been little direct observational evidence that would favor any particular physical mechanism. From our wide-field study of the spatial distribution of E+A and other types of spectrally classified galaxies in MACSJ0717.5+3745, we believe to have found the strongest evidence to date for ram-pressure stripping being the most effective, and in fact possibly only, mechanism driving the rapid evolution of E+A galaxies in clusters⁷. This is because almost all of the E+A galaxies in the MACSJ0717.5+3745 system are found to lie, in projection, near the cluster core⁸ and within the ram-pressure stripping radius R_{rs} . Simulations (e.g. (Tonnesen et al. 2007)) show that ram-pressure stripping is the most efficient mechanism to remove the gas in the galaxies, and, therefore, to terminate star formation. Furthermore, the complex substructure in both X-ray emission (Fig. 1) and galaxy density (Fig. 7) makes MACSJ0717.5+3745 a perfect representative of a the kind of cluster merger explored in the numerical simulation of Fujita et al. (1999). The latter authors find that the ram-pressure on galaxies near the cluster core increases dramatically as clusters collide, and that cluster mergers also bring many blue galaxies near the cluster center – the combination of these two effects leads to an increase in the fraction of post-starburst galaxies increases in the cluster core. The results of our study firmly rule out galaxy mergers as the primary driver for the creation or evolution of E+A galaxies. If galaxy mergers were responsible for the termination of star formation in E+A galaxies, we would expect to see their distribution peak in regions where the galaxy densities and relative velocities are most conducive to mergers, i.e., group-like environments and the cluster infall region itself. This is clearly inconsistent with the results presented in §5.6 (Figs. 12 and 14). The less violent galaxy-galaxy interaction mechanisms harassment and starvation are ruled out too, not only because they cannot explain the observed concentration of E+A galaxies near the regions of steeply increasing intra-cluster gas density, but also because they act over effective time scales (Treu et al. 2003) of several billion years and are thus too slow to sharply terminate the star formation in E+A galaxies. By contrast, the time (Treu et al. 2003) needed for a galaxy to fall from the virial radius, where star formation would be triggered, to the ram-pressure stripping radius, where the star formation would be terminated again essentially instantaneously, and then on to the cluster core (~ 1 Gyr) is well matched to the lifetime of the E+A phase (~ 1 Gyr). We note though that galaxy mergers are not ruled out in terms of effective time scale (a few hundreds million years) as a mechanism for the creation of E+A galaxies in general. In the field mergers appear indeed to be

⁷ Note that we refer here to the extreme E+A galaxies as defined by our strict criteria of Balmer line absorption. We do not rule out the possibility that other physical mechanisms play a significant role in the evolution of post-starburst galaxies with weaker Balmer absorption lines.

⁸ Although spurious trends could conceivably be introduced into the observed spatial distribution if all or most of our E+A galaxies were in fact dust-enshrouded emission-line galaxies (Smail et al. 1999; Sato & Martin 2006), it is difficult to imagine reasons for which any dust-extinction patterns should correlate this closely with cluster radius.

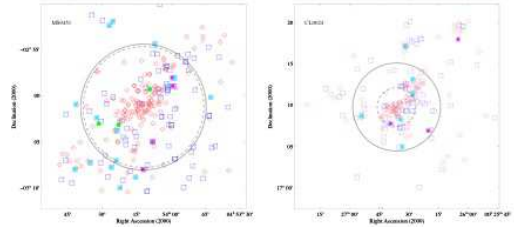


FIG. 15.— Spatial distribution of different galaxy types in MS0451.6–0305 and Cl0024+16 based on data from Moran et al. (2007). The symbols are the same as in Fig. 12. The solid circle has radius R_{vir} , whereas the dashed circle marks R_{rs} as shown in Figure 1 of Moran et al. (2007). [The full resolution figure will be published in ApJ]

the dominant mechanism (Zabludoff et al. 1996; Yang et al. 2004; Goto et al. 2003; Tran et al. 2004). This dichotomy between the origin of E+A galaxies in low- and high-density environments has previously been suggested by Tran et al. (2003) and Tran et al. (2004).

6.4. Comparison to Other Clusters

To test whether our conclusions extend beyond MACSJ0717.5+3745, we investigate the distribution of E+A galaxies in the only two other clusters at intermediate redshift for which spectroscopic data of comparable quality are available over a similarly large field of view, namely MS0451.6–0305 and Cl0024+16⁹(Treu et al. 2003; Moran et al. 2007). Although the details of their survey in Moran et al. (2007), such as the selection criteria, the magnitude limit, the instrumental setup, and the technical details of the EW measurements¹⁰, are different from those of our work, a qualitative comparison should still be permitted. In addition, we attempt a comparison between MACSJ0717.5+3745 and a similarly massive cluster in the local universe, to test whether the spatial distribution of E+A galaxies is consistent. This would imply that, regardless of any redshift evolution in the relative prevalence of galaxies of a given spectroscopic type, ram-pressure stripping is the sole physical mechanism driving the evolution of E+A galaxies in clusters at all epochs. Since E+A galaxies are rare in local clusters we are left with a single system featuring enough E+A galaxies for a statistically meaningful comparison, the Coma cluster(Poggianti et al. 2004).

MS0451.6–0305 ($z = 0.54$, $L_x = 17 \cdot 10^{44}$ ergs s^{-1} , $T_x = 7$ keV, Gioia & Luppino 1994, Ebeling et al. 2007) is comparable to MACSJ0717.5+3745 in that it is one of the most X-ray luminous and best-studied clusters at $z \sim 0.5$. Unlike MS0451.6–0305 and MACSJ0717.5+3745, Cl0024+16 ($z = 0.39$) is an optically selected cluster and much less X-ray luminous ($L_x = 2.9 \cdot 10^{44}$ ergs s^{-1} , $T_x = 3.5$ keV, Zhang et al. 2005). We nonetheless include here for comparison purposes to investigate the relevance of cluster properties such as total mass, dynamical state, and core density. The Coma cluster, our local reference, is the most massive cluster at $z < 0.05$ ($T_x = 9.0$ keV (Donnelly et al. 1999).

As shown in Fig. 15, E+A galaxies are rare in both MS0451.6–0305 ($1_{-0.6}^{+1.1}\%$) and Cl0024+16 ($0_{-0}^{+0.7}\%$) com-

⁹ EW measurements for these systems were obtained from <http://www.astro.caltech.edu/~smm/clusters/>.

¹⁰ Moran et al. (2007) adopt the Lick system(Worthey et al. 1994) for their EW measurements; we perform our spectral classification using their $H\delta_A$ and $H\gamma_A$ values. Although use of the Lick-system results will affect our classification to some extent, we expect the differences to be insignificant comparing to other systematic uncertainties.

pared to MACSJ0717.5+3745 ($3.2^{+1.0}_{-0.8}\%$), although the uncertainties are large. However, their spatial distribution (all within R_{rs}) is consistent with what we observe in MACSJ0717.5+3742. In addition, the fact that the E+A galaxies in MS0451.6–0305 avoid the dense cluster core lends support to the hypothesis (see §5.5) that the true three-dimensional spatial distribution of this type of galaxies resembles a shell inside the ram-pressure stripping radius. No E+A galaxy at all is found in Cl0024+16. However, as reflected in its much smaller ram-pressure stripping radius, this cluster is much less massive than either of MS0451.6–0305 and MACSJ0717.5+3745. In fact, the density of this cluster’s core region is still likely to be overestimated because of the unusual geometric and dynamical properties of Cl0024+16, which is known to be a high-velocity merger along our line of sight (Kzoske et al. 2002).

Our results for MACSJ0717.5+3742 are consistent with the distribution of e(a)/e(b) galaxies in MS0451.6–0305 and Cl0024+16, too. In either cluster, these starburst candidates are distributed much more widely than the E+A or absorption-line population.

The spatial distribution of E+A galaxies in Coma (Poggianti et al. 2004) is also consistent with our result¹¹. Poggianti et al. (2004) separate E+A galaxies into two categories according to their color. Based on the relative position of the red sequence and the E+A galaxies in Fig. 9, the E+A galaxies in MACSJ0717.7+3745 mostly belong to the class of “blue E+A” galaxies, which Poggianti et al. (2004) find to be concentrated near the core of Coma. A similar sub-population is selected by focusing on the “extreme” E+A galaxies with $H_\delta > 6\text{\AA}$ (see also §4.3). Applying this criterion to the k+a sample of Poggianti et al. (2004) we again find most of them (7 out of 9) to be located near the cluster center but avoiding the very core. Finally, Poggianti et al. (2004) speculate that the distribution of these youngest E+A galaxies in Coma traces the X-ray substructure, suggesting that the origin of these extreme E+A galaxies may be related to merger-induced shocks in the cluster gas. While, qualitatively, this picture is not in conflict with our findings for MACSJ0717.7+3745, a known major merger (Fig. 1 shows the complex X-ray morphology of the cluster core), this hypothesis would make the absence of E+A galaxies in Cl0024+16 even harder to explain.

7. CONCLUSION

MACSJ0717.5+3745 is a very X-ray luminous cluster at $z = 0.55$ which shows complex sub-cluster and filamentary structure in both X-ray surface brightness and galaxy density. Along the filament, we detect a significant offset in the average redshift of galaxies, corresponding to $\sim 630\text{km s}^{-1}$ in velocity, as well as a decrease in velocity dispersion from the core of the primary cluster to the end of filament. These variations are likely a combination of spatial (Hubble flow) and kinematic effects (peculiar velocities) in this highly disturbed, merging system; a detailed analysis and discussion of the three-dimensional geometry and dynamics of MACSJ0717.5+3745 will be presented in a forthcoming paper.

Using the spectroscopic data obtained by us, primarily with the DEIMOS spectrograph on the KECK-II telescope, we perform an extensive analysis of the spatial distribution of galax-

ies of different spectroscopic types, from the cluster core to the cluster outskirts and the connected linear filament. The spectroscopic sample is selected using blue and red color cuts defined relative to the empirical cluster red sequence in the V and R_c bands. The final spectroscopic catalog is more than 70% complete at $R_c < 21.75$. The applied blue color cut causes the number of emission-line galaxies in this structure, in particular the starburst galaxies, to be underestimated – our analysis of the spatial distribution of the cluster members of various spectroscopic types should, however, not be affected.

We classify cluster members into emission-line, absorption-line, and E+A galaxies using the strength of the [OII] and H_β emission lines, as well as the absorption features H_δ and H_γ . The emission-line galaxies are further categorized into the subtypes e(a), e(b), and e(c), depending on the strengths of the [OII] emission- and H_δ absorption-line features. We emphasize that in order to eliminate contamination from absorption- or emission-line galaxies, we adopt a very strict criterion for our definition of E+A galaxies, namely $\frac{(H_\delta + H_\gamma)}{2} > 6\text{\AA}$, and also require the absence of [OII] and H_β emission. The location of these E+A galaxies in color-magnitude and color-color diagrams confirms that they represent the transition phase between emission-line galaxies, in particular the e(a) and e(b) sub-types, and absorption-line galaxies.

The main result of this study is that E+A galaxies are found to reside almost exclusively within the ram-pressure radius of the cluster. Since E+A galaxies are not observed in significant numbers in other regions of this system where the local galaxy density is similarly high, and since the relatively high galaxy velocities near the ram-pressure radius are unfavourable for galaxy mergers, we conclude that galaxy-gas interactions, rather than galaxy mergers, are likely the dominant mechanism for the evolution of the E+A galaxies, at least in clusters at intermediate redshift. Our interpretation that the star formation in these galaxies is terminated because the gas reservoir is being stripped away by the intra-cluster medium as galaxies fall into the cluster core is consistent with the results obtained for other two clusters, MS0451.6–0305 and Cl0024+16. E+A galaxies are only found within the ram-pressure radius of MS0451.6–0305, and no E+A galaxies at all are found in Cl0024+16, a low-mass system featuring a very small ram-pressure stripping radius. The large number of E+A galaxies around the core of MACSJ0717.7+3745, compared to the similarly X-ray luminous cluster MS0451.6–0305, can be naturally explained by the significant merger activity in the latter system, an effect that is consistent with the results of numerical simulations.

Although the spatial distribution of E+A galaxies in MACSJ0717.7+3745 shows clear evidence of environmental effects on galaxy evolution in clusters, many issues still need further investigation. Specifically, we need to better understand the role of cluster mergers, and what exactly triggers starbursts as galaxies are falling into the cluster. Both of these questions can be addressed by extending this work to the full sample of the 12 most distant MACS clusters, thereby covering systems of very different dynamical states and a wide range of large-scale environments. For MACSJ0717.7+3745, accurate star-formation rates measured from infrared data obtained with Spitzer will help greatly in this regard. In addition we aim to use galaxy morphologies and deep X-ray observations to study in detail the gas-galaxy interactions which we suspect to be responsible for the termination of star formation activity and thus the creation of

¹¹ The study of Poggianti et al. (2004) addresses properties of k+a galaxies selected based on H_δ and [OII]; although this definition is different from ours, the selected galaxy type is similar to our E+A galaxies.

E+A galaxies in clusters.

We thank Leif Wilden and Glenn Morris of Stanford University for assistance with the photometric calibration of our SuprimeCam data for MACSJ0717.7+3745 and the anonymous referee for advice and suggestions that helped to improve this paper. Financial support for this work was provided by the National Aeronautics and Space Administration

through Chandra Award Number GO3-4168X issued by the Chandra X-ray Observatory Center, which is operated by the Smithsonian Astrophysical Observatory for and on behalf of the National Aeronautics Space Administration under contract NAS8-03060. This research has made use of software provided by the Chandra X-ray Center (CXC) in the application packages CIAO, ChIPS, and Sherpa. The analysis pipeline used to reduce the DEIMOS data was developed at UC Berkeley with support from NSF grant AST-0071048.

REFERENCES

- Arnaud, M., Aghnaim, N., & Neumann, D. 2002, *A&A*, 389, 1
- Arnouts, S., Cristiani, S., Moscardini, L. et al. 1999, *MNRAS*, 310, 540
- Balogh, M. L., Navarro, J. F., & Morris, S. L. 2000, *ApJ*, 540, 113
- Balogh, M. L. et al. 2004, *MNRAS*, 348, 1355
- Barger, A. J., Maragon-Salamanca, A., Ellis, R. S., Couch, W. J., Smail, I., & Sharples, R. M. 1996, *MNRAS*, 279, 1
- Barnes, J. E. & Hernquist, L. 1992, *ARAA*, 30, 705
- Barrett, E., 2005, PhD thesis
- Beers, T. C., Flynn, K., & Gebhardt, K. 1990, *AJ*, 100, 32
- Bertin, E. & Arnouts, S. 1996, *A&AS*, 117, 393
- Blake, C., et al. 2004, *MNRAS*, 355, 713
- Blakeslee, J. P., Holden, B. P., Franx, M. et al. 2006, *ApJ*, 644, 30
- Bower, R. G. & Balogh, M. L. 2004, Cluster if Galaxies: Probes of Cosmological Structure and Galaxy Evolution from the Carnegie Observatories Centennial Symposia, 325
- Bruzual, G. & Charlot, S. 2003, *MNRAS*, 344, 1000
- Butcher, H & Oemler, A. Jr. 1978, *ApJ*, 219, 18
- Calzetti, D. 2001, *NewAR*, 45, 601
- Cappellari, M., & Emsellem, E. 2004, *PASP*, 116, 816, 138
- Cavaliere A. & Fusco-Femiano R. 1976, *A&A*, 49, 137
- Cooper, M. C., Newman, J. A., Weiner, B. J., et al. 2007, *ApJ*
- Couch, W. J., & Sharples, R. M. 1987, *MNRAS*, 229, 423
- Cowie, L. L., Songaila, A., Hu, E. M., & Cohen, J. G. 1996, *AJ*, 112, 839
- Czoske, O., Moore, B., Kneib, J.-P., Soucail, G. 2002, *A&A*, 386, 31
- Donnelly, R. H., Markevitch, M., Forman, W., Jones, C., Churazov, E., & Gilfanov, M. 1999, *ApJ*, 513, 690
- Donovan, D. 2007, PhD thesis
- Dressler, A. 1980, *ApJ*, 236, 351
- Dressler, A. & Gun, J. E. 1983, *ApJ*, 270, 7
- Dressler, A., et al. *ApJ*, 490, 577
- Dressler, A., Smail, I., Poggianti, B. M., Butcher, H., Couch, W. J., Ellis, R. S., & Oemler, A. J. 1999, *ApJS*, 122, 51
- Ebeling, H., Edge, A., & Henry, P. 2001, *ApJ*, 553, 668
- Ebeling, H., Barrett, E., & Donovan, D. 2004, *ApJL*, 609, 49
- Ebeling, H., White, D., & Rangarajan, F. 2006, *MNRAS*, 368, 65
- Ebeling, H., Donovan, D., Ma, C.-J., Edge, A., & van Speybroeck, L. 2007, *ApJL*, 661, 33
- Fisher, D., Fabricant, D., Franx, M., & van Dokkum, P. 1998, *ApJ*, 498, 195
- Fujita, Y., Takizawa, M., Nagashima, M., & Enoki, M. 1999, *PASJ*, 51, L1
- Ghigna, S., Moore, B., Governato, F., Lake, G., Quinn, T., & Stadel, J. 1998, *MNRAS*, 300, 146
- Gioia, I. M., & Luppino, G. A. 1994, *ApJS*, 94, 583
- Gomez, P. L., Nichol, R. C., Miller, C. J., et al. 2003, *ApJ*, 584, 210
- Goto, T., Nichol, R., Miller, C., et al. 2003, *PASJ*, 55, 771
- Goto, T. 2006, *MNRAS*, 369, 1765
- Goto, T. 2007, *MNRAS*, 381, 187
- Gunn, J. E. & Gott, J. R. III 1972, *ApJ*, 176, 1
- Hogg, D. W., Masjedi, M., Berlind, A. A., Blanton, M. R., Quintero, A., D., & Brinkmann, J. 2006, *ApJ*, 650, 763
- Ilbert, O., Arnouts, S., & McCracken, H., et al. 2006, *A&A*, 457, 841
- Kartaltepe, J., Ebeling, H., Ma, C.-J., Donovan, D., Barrett, E. in preparation
- Kauffmann, G. et al. 2003, *MNRAS*, 341, 33
- Kewley, L., Groves, B., Kauffmann, G., & Heckman, T. 2006, *MNRAS*, 372, 961
- Kodama, T, Smail, I, Nakata, F., Okamura, S., & Bower, R. G. 2001, *ApJL*, 562, 9
- Larson, R. B., Tinsley, B. M., & Caldwell, C. N. 1980, *ApJ*, 237, 692
- Lewis, I., Balogh, M., De Propris, R., et al. 2003, *MNRAS*, 334, 673
- Marcillac, D., Rigby, J., Rieke, G., & Kelly, D. 2007, *ApJ*, 654
- Maughan B.J., Jones L.R., Ebeling H., Perlman E., Rosati P., Frye C., Mullis C.R. 2003, *ApJ*, 587, 589
- Mewe, R., Gronenschild, E.H.B.M., & van den Oord, G.H.J. 1985, *A&AS*, 62, 197
- Miyazaki S. et al. 2002, *PASJ*, 54, 833
- Moustakas, J., Kennicutt, R. C., & Tremonti, C. A. 2006, *ApJ*, 642, 775
- Moore, B., Katz, N, Lake, G, Dressler, A, & Oemler, A 1996, *Nature*, 379, 613
- Moore, B., Lake, G., & Katz, N. 1998, *ApJ*, 1007
- Moran, S., Ellis, R., Treu, T., Salim, S., Rich, R. M., Smith, G. P., & Kenib, J.-P. 2006, *ApJL*, 641, 97
- Moran, S., Ellis, R., Treu, T., Smith, G., Rich, R., & Smail, I. 2007, *ApJ*, 671, 1503
- Oemler, A. Jr. 1974, *ApJ*, 194, 1
- Poggianti, B. M., Smail, I, Dressler, A, Couch, W. J., Barger, A. J., Butcher, H, Ellis, R. S., & Oemler, A., Jr. 1999, *ApJ*, 518, 576
- Poggianti, B. M., & Wu, H. 2000, *ApJ*, 529, 157
- Poggianti, B., Bridges, T., Komiyama, Y., et al. 2004, *ApJ*, 601
- Poggianti, B., von der Linden, A., De Luccia, G., et al. 2006, *ApJ*, 642
- Postman, M. et al. 2005, *ApJ*, 623, 721
- Quintero, A. D., Hogg, D. W., & Blanton, M. R. 2004, *ApJ*, 602
- Ruderman, J., & Ebeling, H. 2005, *ApJL*, 623, L81
- Sato, T., & Martin, C. 2006, *ApJ*, 647
- Smail, I., Morrison, G., Gray, M. E., Owen, F. N., Ivison, R. J., Kneib, J.-P., & Ellis, R. S. 1999, *ApJ*, 525, 609
- Smith, G. P., Treu, T., Ellis, R. S., Moran, S. M., & Dressler, A. 2005, *ApJ*, 620, 78
- Tonnesen, S., Bryan, G. L., & van Gorkom, J. H. 2007, *ApJ*, 671, 1434
- Tran, K-V, Franx, M., Kelson, D., & van Dokkum, P. 2003, *ApJ*, 599
- Tran, K-V, Franx, M., Illingworth, G., van Dokkum, P., Kelson, D., & Magee, D. 2004, *ApJ*, 609
- Tran, K-V., van Dokkum, P., Illingworth, G., Kelson, D., Gonzalez, A., & Franx, M. 2005, *ApJ*, 619, 134
- Tran, K-V., Franx, M., Illingworth, G., van Dokkum, P., Kelson, D., Blakeslee, J., & Postman, M. 2007, *ApJ*, 661
- Treu, T., Ellis, R., Kneib, J., Dressler, A., Smail, I., Czoske, O., Oemler, A., & Nararajan, P. 2003, *ApJ*, 591
- Worthey, G., Faber, S. M., Gonzalez, J.J., & Burstein, D. 1994, *ApJS*, 94, 687
- Yagi, M., Goto, T. & Hattori, T. 2006, *ApJ*, 642, 152
- Yan, R., Newman, J., Faber, S., Konidris, N., Koo, D., & Davis, M. 2006, *ApJ*, 648, 281
- Yang, Y, Zabludoff, A. I., Zaritsky, D., Lauer, T. R., & Mihos, J. C. 2004, *ApJ*, 607, 258
- Zabludoff, A. I., et al. 1996, *ApJ*, 466, 104
- Zhang, Y. Y., Bohringer, H., Mellier, Y., Soucail, G., & Forman, W. 2005, *A&A*, 429, 85